Fractal structures in the parameter space of nontwist area-preserving maps

A. C. Mathias,[1] M. Mugnaine,[1] M. S. Santos,[1] J. D. Szezech Jr.,[2] I. L. Caldas,[3] and R. L. Viana[1,*]

[1]*Departamento de Física, Universidade Federal do Paraná, Curitiba, Paraná 81531-980, Brazil*

[2]*Departamento de Matemática e Estatística, Universidade Estadual de Ponta Grossa, Ponta Grossa, PR 84030-900, Brazil*

[3]*Departamento de Física Aplicada, Instituto de Física da Universidade de São Paulo, São Paulo, SP 05508-090, Brazil*

(Received 8 July 2019; published 18 November 2019)

Fractal structures are very common in the phase space of nonlinear dynamical systems, both dissipative and conservative, and can be related to the final state uncertainty with respect to small perturbations on initial conditions. Fractal structures may also appear in the parameter space, since parameter values are always known up to some uncertainty. This problem, however, has received less attention, and only for dissipative systems. In this work we investigate fractal structures in the parameter space of two conservative dynamical systems: the standard nontwist map and the quartic nontwist map. For both maps there is a shearless invariant curve in the phase space that acts as a transport barrier separating chaotic orbits. Depending on the values of the system parameters this barrier can break up. In the corresponding parameter space the set of parameter values leading to barrier breakup is separated from the set not leading to breakup by a curve whose properties are investigated in this work, using tools as the uncertainty exponent and basin entropies. We conclude that this frontier in parameter space is a complicated curve exhibiting both smooth and fractal properties, that are characterized using the uncertainty dimension and basin and basin boundary entropies.

DOI: 10.1103/PhysRevE.100.052207

I. INTRODUCTION

Fractal structures appear very often in the analysis of many nonlinear dynamical systems, both conservative and dissipative [1]. In the latter, for example, the boundaries between basins of different attractors can be fractal [2,3], and the attractors themselves may have fractal dimensions, even when nonchaotic [4]. The existence of fractal boundaries has been also found in open Hamiltonian (conservative) systems, for the boundary between escape (or exit) basins [5]. This is the case, for example, of chaotic scattering [6]. One of the observable consequences of the existence of fractal structures in phase space is final-state sensitivity, i.e., small uncertainties in the initial conditions may lead to large uncertainties with respect to the future behavior of the system [3].

The above-mentioned examples refer to fractal boundaries in phase space. However, fractal boundaries have also been investigated in the parameter space of dissipative systems. Moon has studied the parameter space of a forced nonlinear oscillator with a two-well potential, showing that the boundary between periodic and chaotic motions has a fractal dimension of 1.26 [7]. Another example is the structure of Arnold tongues in the parameter space of the sine-circle map, where the fractal structure of mode locking regions leads to a devil's staircase [8]. In these cases, since the parameter values are known up to some uncertainty, the final state of the system can be difficult to determine.

In spite of its importance, the study of fractal boundaries in the parameter space of conservative (area-preserving) systems has not yet been considered, to our knowledge. We conjecture that this is so because the absence of attractors makes it difficult to achieve a precise characterization of a few common behaviors that could be associated with specified parameter values. The well-known Chirikov-Taylor standard map, which is the paradigm example of area-preserving systems, has only one relevant parameter [9]. This is also the case of the Hénon-Heiles Hamiltonian [10,11].

More complicated conservative systems do have more than one parameter, though, and the question arises of whether or not fractal boundaries exist in their parameter spaces. We address this question in the present paper, offering as a representative example the so-called standard nontwist map (SNTM), introduced by del Castillo-Negrete and Morrison in 1993 [12]. This map models a variety of interesting physical phenomena, like the magnetic field lines in toroidal plasma devices, like tokamaks, with reversed magnetic shear [13,14], and transport by traveling waves in zonal flows with nonmonotonic velocity profiles [15,16].

The violation of the twist property in SNTM leads to the existence of a shearless invariant curve, which acts as a barrier separating chaotic regions in the phase space [15,16]. This internal transport barrier creates two different behaviors, namely the escape of trajectories to plus or minus infinity [17]. The parameter space of the standard nontwist map presents an involved boundary between these behaviors [15].

Our work is a numerical investigation of the parameter space structure of open conservative systems, using a relatively simple example (the SNTM) to illustrate our ideas. However, open conservative systems do appear in many fields of physics, like celestial mechanics (motion in a Hénon-Heiles galactic potential [18], Sitnikov problem [19]), atomic physics (ionization of hydrogen atoms in crossed electric and magnetic fields [20]), and plasma physics (escape of magnetic

*Corresponding author: viana@fisica.ufpr.br

field lines in plasma confinement schemes [21] and in the $\mathbf{E} \times \mathbf{B}$ motion of charged particles subjected to drift waves [22]), among others.

In this work we aim to investigate the geometry of this boundary in the parameter space of the SNTM and the quartic nontwist map. From a cursory inspection it seems to be a fractal curve, due to an evident self-similarity, but a detailed analysis shows that it has both smooth and fractal pieces. The latter are quantitatively investigated by computing its box-counting dimension using the uncertain fraction method [2,3]. We also use the recently developed concepts of basin entropy and basin boundary entropy to characterize the degree of uncertainty related to the fractality of the parameter space region, as well as its boundary [23,24]. This method has been used to investigate escape basins in several dynamical systems of physical interest, like the motion of a charged particle in a magnetic field and electrostatic waves [22], the magnetic field line structure in a tokamak with chaotic limiter [25], and nanoelectromechanical beam resonators actuated by two-sided electrodes [26].

This paper is organized as follows: in Sec. II we introduce the SNTM and some of its dynamical properties, chiefly the existence of a shearless invariant curve in phase space. In Sec. III we consider the type of boundary present in the parameter space of the SNTM and how it influences the final behavior of the system trajectories. Section IV is devoted to a classical analysis of the fractality of this boundary using the uncertainty exponent technique. We also show the results of the basin entropy and basin boundary entropy for this boundary. The last section contains our Conclusions.

II. STANDARD NONTWIST MAP

The standard nontwist map (SNTM) was proposed and defined in Ref. [12]:

$$x_{n+1} = x_n + a\left(1 - y_{n+1}^2\right), \tag{1}$$

$$y_{n+1} = y_n - b\,\sin(2\pi x_n), \tag{2}$$

where $x \in [-1/2, 1/2)$ and $y \in \mathbb{R}$ are coordinates in the phase space $\mathbb{T} \times \mathbb{R}$, and $a \in (0, 1)$ and $b \in \mathbb{R}$ are parameters of the system. This map is area preserving and violates the twist condition $|\partial x_{n+1}/\partial y_n| \geqslant c > 0$, where c is a real number, for all (x, y) along a curve in phase space. The SNTM violates the twist condition along an invariant curve in phase space called shearless curve [15].

In both sides of the shearless invariant curve there are chains of periodic orbits of the same rotation number. This is illustrated in the phase spaces of the SNTM depicted in Figs. 1(a) and 1(b), where the value of b is kept fixed at 0.6 and the value of a is slightly increased from 0.358 to 0.365. The shearless curve is the red curve which separates periodic island chains. As the parameter a increases these islands coexist with chaotic orbits, which eventually engulf practically all islands. If the shearless invariant curve is not broken, however, these two chaotic regions do not mix their orbits [Fig. 1(c)]. For other parameter values this barrier breaks down and a chaotic orbit becomes able to explore a broader region of the phase space [Fig. 1(d)].

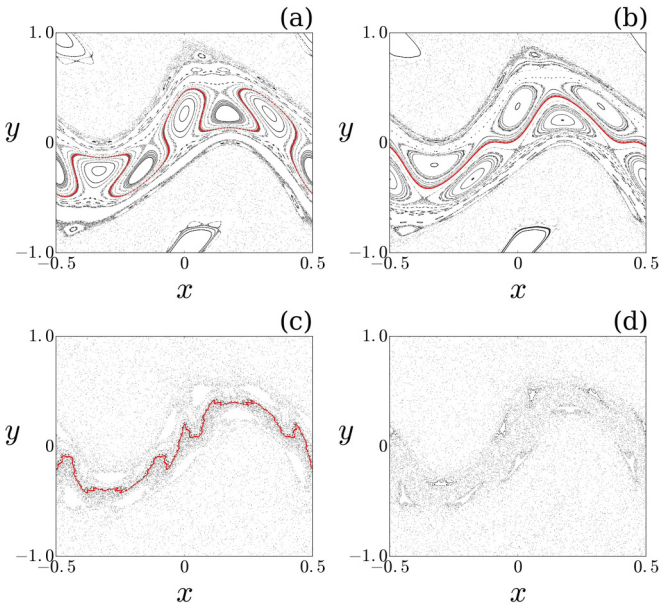

FIG. 1. Phase spaces of the SNTM for (a) $a = 0.358$ and $b = 0.6$, (b) $a = 0.365$ and $b = 0.6$, (c) $a = 0.455$ and $b = 0.797$, and (d) $a = 0.455$ and $b = 0.851$. The red line in phase spaces (a), (b), and (c) is the shearless curve.

After the shearless curve breakup a given initial condition generates a chaotic orbit, except if it is located inside a periodic island remnant. This chaotic orbit has two asymptotic behaviors: it either escapes to plus or minus infinity. This fact can be illustrated by the corresponding escape (or exit) basins. Such a basin is defined by the set of initial conditions, in the phase space, that generates orbits that escape through a specified exit [5]. Numerically we consider two horizontal lines in phase space, namely $\mathbf{A} : (-1/2 \leqslant x < 1/2, y = -1)$ and $\mathbf{B} : (-1/2 \leqslant x < 1/2, y = 1)$. Once a given initial condition crosses $\mathbf{A}$ ($\mathbf{B}$) the subsequent trajectory asymptotes to minus (plus) infinity.

Accordingly the escape basins, denoted as $\mathcal{B}_n(\mathbf{A})$ and $\mathcal{B}_n(\mathbf{B})$, are the sets of initial conditions that generate orbits that, after a certain time n, cross the lines at $y = -1$ or $y = 1$, respectively. If n is suitably chosen, it turns out that the changes in the escape basins are negligible. On the other hand, even after this time n, there can still exist orbits that do not escape, if they are trapped within periodic islands or because the remnants of the shearless curve act as a partial barrier for the transport of these trajectories [27]. This partial barrier can also be called "shearless Cantori," as proposed by Blazevski and del-Castillo-Negrete as a nontwist version of the cantori [28]. The corresponding initial conditions form a set of no escape.

The escape basins of the SNTM through the exits labeled as $\mathbf{A}$ and $\mathbf{B}$ are depicted in Fig. 2 as green and red regions, respectively. The parameter values used in Fig. 2 are the same as in Fig. 1. The escape basins are separated by the shearless curve as far as it has not been broken [Figs. 1(a)–1(c)]. In these cases, while the escape basins $\mathcal{B}_n(\mathbf{A})$ and $\mathcal{B}_n(\mathbf{B})$ appear to be connected sets, the set of no escape (white points) is formed by the union of many disjoint sets, basically remnants of periodic islands partially engulfed by the chaotic orbits.

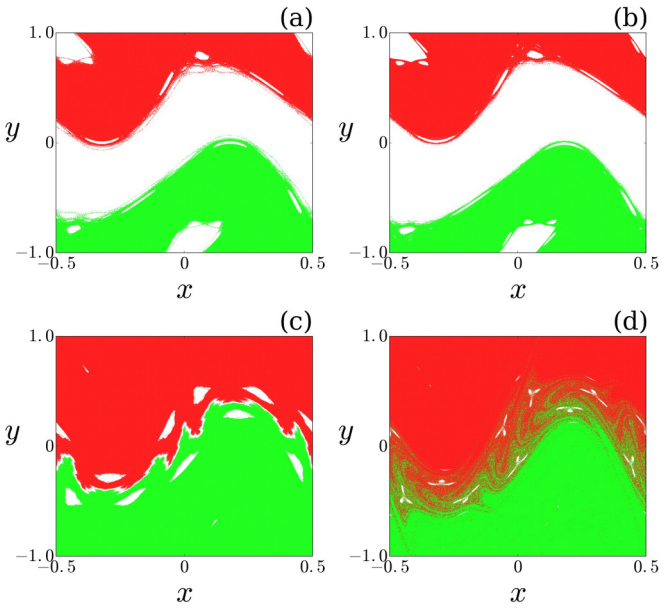

FIG. 2. Escape basins of the SNTM for (a) $a = 0.358$ and $b = 0.6$, (b) $a = 0.365$ and $b = 0.6$, (c) $a = 0.455$ and $b = 0.797$, and (d) $a = 0.455$ and $b = 0.851$. The green and red basins represent the set of initial conditions that escape through the exits $\mathbf{A} : y = -1$ and $\mathbf{B} : y = 1$, respectively. The initial conditions that do not escape within $n = 10^4$ map iterates are depicted in white. We used a grid of $10^3 \times 10^3$ initial conditions.

After the shearless curve has been broken, the escape basins are intertwined therein, with fingerline striations characteristic of fractal sets. Indeed, the analysis of the escape basins of the SNTM has revealed a fractal structure [29].

III. PARAMETER SPACE OF THE STANDARD NONTWIST MAP

The breakup of the shearless invariant curve occurs for determined values of the parameters a and b. It is thus worthwhile to investigate, in terms of the respective parameter space (a, b), which parameter values lead to shearless curve breakup and how they are separated from the other ones. We can determine this boundary using a method proposed by Shinohara and Aizawa [30], consisting in using indicator points that are fixed points of the lines of symmetry of the SNTM, given by [31]

$$z_1^{(\pm)} = \left(\pm\frac{1}{4}, \pm\frac{b}{2}\right), \quad z_2^{(\pm)} = \left(\frac{a}{2} \pm \frac{1}{4}, 0\right). \tag{3}$$

The construction of parameter space is obtained as follows: we cover a parameter plane region (such as $0 < a < 1$ and $0 < b < 1$) with a fine mesh of $N_p \times N_p$ points. For each pair of parameters (a, b) we used the four indicator points, given by (3), as initial conditions, and iterate them a long time, e.g., $n = 10^6$ iterations. If the y value of the corresponding trajectory stays below a specified threshold, e.g., $|y| < 20$, it is assumed that the shearless curve exists and the point (a, b) is plotted; otherwise, it is not plotted [17].

Our results, using the indicator points (3), are depicted in Fig. 3 for the SNTM. The points in magenta represent

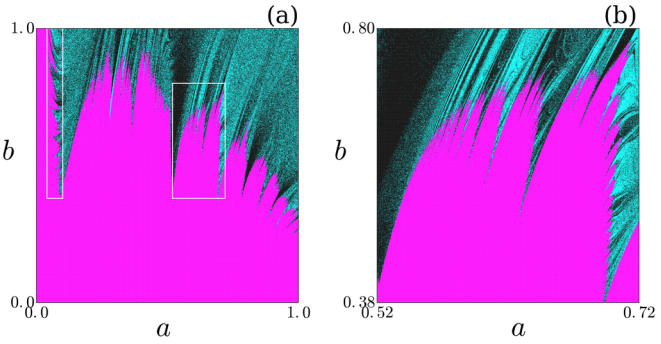

FIG. 3. (a) Parameter space of the standard nontwist map. The magenta points represent the existence of the shearless curve after $n = 10^6$ iterates of the indicator points (3). Black and cyan points represent parameter values for which orbits escape through the exits $y = -1$ and $y = 1$, respectively. Panel (b) is a zoom of the rectangle indicated in the right of (a).

parameter values (a, b) for which there is a shearless invariant curve, the remaining points representing parameter values for which the shearless curve has been broken. In addition, the latter region can be further divided into a set of parameter values (in black) which generates an orbit which escapes through the exit $\mathbf{A} : y = -1$, whereas the points in cyan are parameters for which an orbit escapes through $\mathbf{B} : y = +1$. As we have seen before, the no-escape region is negligibly small after the shearless curve has been broken [see Fig. 1(d) for an example].

A cursory inspection of Fig. 3 suggests that the boundary $\partial\mathcal{B}$ between the parameter regions for which a shearless invariant curve exists (magenta) and does not exist is self-similar and has a fractal structure. The same can be said of the boundary between the parameter regions for which the escape is to plus infinity (cyan) and minus infinity (black). Actually the boundary $\partial\mathcal{B}$ cannot be completely fractal, since there are smooth parts of it corresponding to bifurcation curves, as shown by Wurm *et al.* (see Fig. 11 of Ref. [32], where the bifurcation curves are represented by colored lines superimposed to the numerically determined boundary). These bifurcation curves contain the parameter values a and b for the threshold of collision of periodic orbits with a fixed winding number [32].

The coexistence of smooth and fractal parts of the boundary $\partial\mathcal{B}$ depicted in Fig. 3 is well known in dissipative systems, where it has been long observed that basin boundaries in phase space have different properties in different regions. Many examples have been given by Grebogi and co-workers, who found such behavior in the basin boundary of the kicked double rotor, where there are smooth and fractal regions. Moreover, these different regions are intertwined on arbitrarily fine scales [33]. Hence it is virtually impossible to separate smooth and fractal regions on the same boundary.

Let us now focus our attention in the fractal part of the boundary $\partial\mathcal{B}$ between magenta and cyan+black regions in Fig. 3. In the left-hand side of it there is a deep tongue that is anchored at $a \approx 0.1$, which separates the boundary into a left-hand side and the right-hand side, hereafter denoted by $\partial\mathcal{B}_{\text{left}}$ and $\partial\mathcal{B}_{\text{right}}$, respectively, which seem to be qualitatively different, an impression that our further analysis will prove

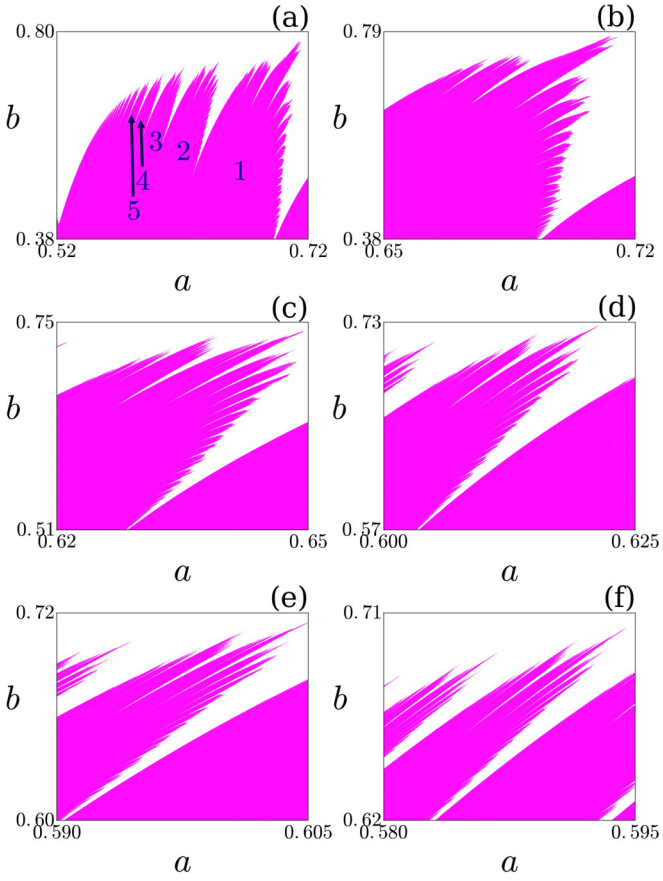

FIG. 4. (a) Region, in the parameter spaces of the SNTM, for which the shearless curve exists (magenta points). White points represent parameter values for which the orbits escape to plus or minus infinity. (b)–(f) A sequence of magnifications of the regions specified by numbers (1)–(5) in (a).

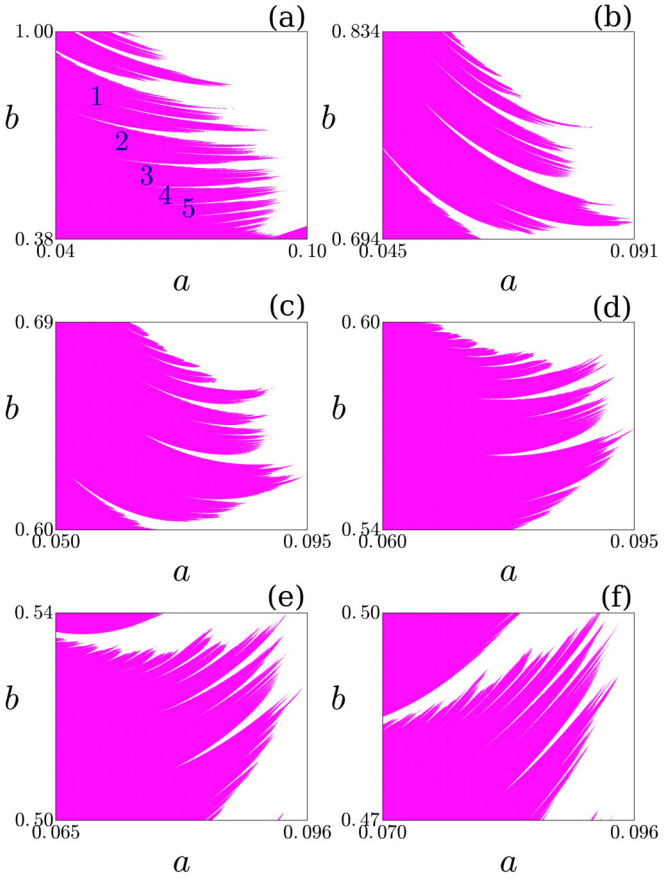

FIG. 5. (a) Second region, in the parameter spaces of the standard nontwist map, for which the shearless curve exists (magenta points). White points represent parameter values for which the orbits escape to plus or minus infinity. (b)–(f) A sequence of magnifications of the regions specified by numbers (1)–(5) in (a).

wrong. A glimpse of the complexity of the boundary parts $\partial\mathcal{B}_{\text{right}}$ and $\partial\mathcal{B}_{\text{left}}$ is provided by the various magnifications shown in Figs. 4 and 5, respectively. These magnifications are representative since in each of them there is a tonguelike structure, for which the left part is fractal and the right part is smooth.

In Figs. 4(b)–4(f), which focus on the boundary part $\partial\mathcal{B}_{\text{right}}$, we show magnifications of the regions labeled as 1 to 5 in Fig. 4(a). Figure 5 does the same, but for the boundary part $\partial\mathcal{B}_{\text{left}}$. While in both cases a self-similar structure is evident, it cannot be said that their fractal properties are identical. This requires a quantitative analysis to be performed in the next section.

Due to the violation of the nontwist condition, the SNTM presents more than one orbit of the same winding number. The variation of parameters can lead to the collision and annihilation of these orbits [32,34]. The parameter values (a, b) for which there is a collision of periodic orbits form a bifurcation curve in the parameter space, first defined by del Castillo-Negrete, Greene, and Morrison in Ref. [15]. From the latter reference, the construction of these curves has been established and the superposition of them in the parameter space was published by Wurm and co-workers (see Fig. 11 of Ref. [32]), showing that the bifurcation curves follow the smooth parts of the boundary in the parameter space. This bifurcation scenario has been also investigated by Petrisor *et al.* [35].

IV. UNCERTAINTY FRACTION AND BASIN ENTROPIES

In this work we present two different quantitative characterizations of the boundary $\partial\mathcal{B}$ and its two parts, in parameter space. The first is the computation of the box-counting dimension of $\partial\mathcal{B}$ by the uncertainty fraction method [2,3]. The second is the determination of the so-called basin entropy and basin boundary entropy to quantify the degree of uncertainty due to the fractality of the boundary $\partial\mathcal{B}$ [23,24].

The basics of the uncertainty fraction method are well known but we will outline them here since in most cases the boundaries are in phase space, rather than in parameter space. We start from a parameter space region, like that depicted in Fig. 3, and consider a large number (we choose 10^3) of randomly chosen parameter pairs (a, b). For each parameter pair we iterate the SNTM using, as initial conditions, the first pair of indicator points given by (3), with the upper signs. After a long time (10^6 map iterations) we test whether or not the trajectory has crossed either of the two threshold lines ($|y| = 20$): if so, we assume that the shearless curve has been

TABLE I. Basin entropy S_b, basin boundary entropy S_{bb}, and box-counting dimension d of the boundary piece $\partial\mathcal{B}_{\text{left}}$ in the parameter space of the SNTM. The numbers (1) to (5) refer to the magnifications shown in Fig. 5.

$\partial\mathcal{B}_{\text{left}}$	1	2	3	4	5
S_b	0.048 ± 0.010	0.040 ± 0.009	0.043 ± 0.008	0.066 ± 0.013	0.062 ± 0.012
S_{bb}	0.435 ± 0.028	0.457 ± 0.032	0.445 ± 0.028	0.436 ± 0.030	0.430 ± 0.028
d	1.815 ± 0.018	1.853 ± 0.024	1.818 ± 0.005	1.873 ± 0.004	1.822 ± 0.027

broken; if not so, we assume that the shearless curve still exists.

Then we perturb the parameter values (a, b) to a second pair (a', b'), chosen randomly inside a small disk of radius ϵ centered at (a, b), i.e., such that $\sqrt{(a-a')^2+(b-b')^2} \leqslant \epsilon$. Then we iterate the map using the second pair of indicator points given by (3) with the lower signs, and repeat the test. If the outcomes turn out to be different we refer to the parameter pair (a, b) as ϵ-uncertain. The uncertain fraction $f(\epsilon)$ is the ratio between ϵ-uncertain parameter pairs and the total number of them. These computations are repeated 10 times for each value of ϵ, which varied from 10^{-1} to about 10^{-10}. The fraction of a pair of uncertain parameters $f(\epsilon)$ is expected to increase with ϵ as a power law $f(\epsilon) \sim \epsilon^{\alpha}$, where α is the so-called uncertainty exponent [2,3].

In analogy with the corresponding treatment for phase space, let D be the parameter space dimension, and let $N(\delta)$ be the minimum number of D-dimensional boxes of length δ necessary to cover the boundary. The box-counting dimension of the latter is $d = \lim_{\delta\to 0} \ln N(\delta)/\ln(1/\delta)$, such that $N(\delta)$ scales as δ^{-d} for small enough δ [1]. If we set $\delta = \epsilon$, the volume of the uncertain region in the parameter space will be $N(\epsilon)$ times the volume of the D-dimensional cubes, which is ϵ^D. Since the pair of parameters are uniformly chosen over the parameter space region, the uncertain fraction is of the order of the total volume $N(\epsilon)\epsilon^D = \epsilon^{(D-d)}$. Thus the uncertainty exponent results in $\alpha = D - d$. In our case we have $D = 2$ for the parameter space, for which $\alpha = 2 - d$, in such a way that a smooth boundary with $d = 1$ has $\alpha = 1$, whereas $0 < \alpha < 1$ characterizes a fractal boundary [2,3].

We computed the uncertainty exponent and the corresponding estimate for the box-counting dimension of the boundary pieces $\partial\mathcal{B}_{\text{left}}$ and $\partial\mathcal{B}_{\text{right}}$, the results being shown in Tables I and II, respectively. The numbers (1)–(5) refer to the magnifications exhibited in Figs. 4 and 5. We have chosen these magnifications to cover chiefly fractal pieces of the boundary, and we obtained for the corresponding box-counting dimensions $\dim(\partial\mathcal{B}_{\text{left}}) = 1.826 \pm 0.027$ and $\dim(\partial\mathcal{B}_{\text{right}}) = 1.790 \pm 0.045$, suggesting that they are both fractal and with the same dimension $d \approx 1.8$. In addition, we computed the box-counting dimension for those parts of the boundary corresponding to the bifurcation curves in parameter space described by Wurm, resulting in $d = 0.978 \pm 0.011$, which is compatible with our assumption that those pieces are smooth curves.

Due to the presence of smooth boundary pieces in both $\partial\mathcal{B}_{\text{left}}$ and $\partial\mathcal{B}_{\text{right}}$, the boundary is most properly characterized as a combination of a smooth and a fractal part. This is in accordance with a conjecture made by Grebogi *et al.* that basin boundaries in phase space can have at most a finite number of possible dimension values for all typical magnifications [33].

Given the complex nature of this boundary, it would be important to use other measures of uncertainty related to its fractality. One such measure is the so-called basin stability, which essentially quantifies the relative area of the basins [36,37]. In this work we use the recently proposed method of basin entropies, which quantifies the degree of uncertainty due to the fractality of basin [23,24]. Here we outline the basics of this technique, applied to the parameter space.

Let us consider the existence of N_{out} outcomes for a trajectory in phase space, once a parameter pair of values, (a, b), is given. We cover a region Ω of the parameter space with a mesh of N boxes of linear size δ, and define an application $C : \Omega \mapsto \mathbb{N}$ relating each parameter value to some outcome in phase space. This application is called by Daza *et al.* a *color* [23]. Each box contains a large number N_p of parameter values which, after map iterations (using the indicator points as initial conditions), lead to different values of a color, from 1 to N_{out}. By considering the colors into each box randomly distributed we associate a probability p_{ij} to the jth color inside the ith box. Assuming that the trajectories are statistically independent the Shannon entropy of each box is

$$S_i = -\sum_{j=1}^{m_i} p_{ij} \log p_{ij}, \tag{4}$$

where m_i is the number of colors inside the ith box, varying from 1 to N_{out}.

If the boxes covering Ω are nonoverlapping the entropy of the parameter space region is $S = \sum_{i=1}^{N} S_i$. The basin

TABLE II. Basin entropy S_b, basin boundary entropy S_{bb}, and box-counting dimension d of the boundary piece $\partial\mathcal{B}_{\text{right}}$ in the parameter space of the SNTM. The numbers (1) to (5) refer to the magnifications shown in Fig. 4.

$\partial\mathcal{B}_{\text{right}}$	1	2	3	4	5
S_b	0.034 ± 0.007	0.046 ± 0.010	0.046 ± 0.009	0.071 ± 0.015	0.058 ± 0.012
S_{bb}	0.428 ± 0.030	0.428 ± 0.029	0.426 ± 0.027	0.441 ± 0.025	0.427 ± 0.034
d	1.788 ± 0.045	1.803 ± 0.037	1.779 ± 0.036	1.792 ± 0.036	1.797 ± 0.030

entropy is the total entropy divided by the total number of boxes N: $S_b = S/N$. The basin entropy quantifies the degree of uncertainty of the basin; that is, for a single basin the basin entropy is zero, meaning zero uncertainty, whereas for N_A equiprobable basins $S_b = \log N_A$, which means a completely randomized basin structure [23]. If we restrict the computation of the basin entropy to the boxes covering the basin boundaries, i.e., to the N_b boxes containing more than one color, we obtain the so-called basin boundary entropy $S_{bb} = S/N_b$. Accordingly, S_{bb} quantifies the uncertainty referring only to the basin boundary. It has been conjectured that, if $S_{bb} > \log 2$, the basin boundary is fractal, but this turns out to be a sufficient but not necessary criterion, i.e., there may be fractal boundaries even if $S_{bb} < \log 2$.

In the case of SNTM considered here, there are just two outcomes for a trajectory obtained from a given parameter pair (a, b): it either escapes to infinity or does not escape at all (after 10^6 map iterations); hence $N_{\text{out}} = 2$. Considering, as before, the parameter space region Ω as the square $\{0 < a < 1, 0 < b < 1\}$, we cover it with a grid of $N \times N$ points, varying the resolution from $N = 100$ to $N = 250$, and with a number of parameter values *per* box N_p varying from 16 to 100. If we denote by n_a the number of points of each box corresponding to the first outcome (existence of shearless curve) and n_b to the second outcome (nonexistence of the shearless curve, leading to escape to infinity), the corresponding probabilities for the ith box are

$$p_{i1} = \frac{n_a}{n_a + n_b}, \quad p_{i2} = \frac{n_b}{n_a + n_b}, \tag{5}$$

and the entropy of the ith box is simply $S_i = -p_{i1} \log p_{i1} - p_{i2} \log p_{i2}$.

Our results for both basin entropy and basin boundary entropy are summarized in Tables I and II, for the region Ω and its magnifications. The corresponding values are $S_b(\partial\mathcal{B}_{\text{left}}) = 0.035 \pm 0.013$ and $S_b(\partial\mathcal{B}_{\text{right}}) = 0.029 \pm 0.015$ for the basin entropy and $S_{bb}(\partial\mathcal{B}_{\text{left}}) = 0.450 \pm 0.032$ and $S_{bb}(\partial\mathcal{B}_{\text{right}}) = 0.426 \pm 0.033$ for the basin boundary entropy. Finally, for the smooth part of the boundary (corresponding to the bifurcation diagram of the indicator points) we obtained $S_b = 0.005 \pm 0.001$ and $S_{bb} = 0.422 \pm 0.028$.

Within the uncertainty of our measurements, the basin entropy and the basin boundary entropy take on the same values for both left and right boundary pieces, namely $S_b \approx 0.032$ and $S_{bb} \approx 0.438$. It is expected that $S_{bb} > S_b$ since the number of boxes containing the boundary is generally less the total number of boxes. Notice also that $S_{bb} < \log 2$, which is the maximum possible value that S_{bb} can have for a smooth boundary. Since we have shown that the box-counting dimension is higher than unity, the left and right boundary pieces are not only fractal but their fractal content can be quantified by the corresponding entropies. These results are consistent with the hypothesis that the boundary pieces $\partial\mathcal{B}_{\text{left}}$ and $\partial\mathcal{B}_{\text{right}}$ in parameter space have similar properties with respect to the uncertainty of the final state in phase space.

We close this section by mentioning that our results do not depend very much on the detailed form of the standard nontwist map. In order to verify this point we considered the immediate generalization, which is the quartic nontwist map (QNTM), which is [38]

$$x_{n+1} = x_n + a\left(1 - y_{n+1}^2 - p y_{n+1}^4\right), \tag{6}$$

$$y_{n+1} = y_n - b \sin(2\pi x_n), \tag{7}$$

where the phase space variables x and y, as well as the parameters a and b, are similar to the SNTM, whereas a new parameter p has been introduced, which is to be varied from 0.0 to about 0.2 to study changes in the dynamics due to the quartic term. By comparing the parameter space of SNTM and QNTM we observe that the boundaries for both maps are similar, although a slight increase in the size of the chaotic layer bordering both dimerized island chains is visible. Moreover, variations in the value of the parameter p can displace the boundary in parameter space for which the shearless curve breaks down.

V. CONCLUSIONS

There are fractal structures both in the phase space and the parameter space of conservative dynamical systems. While the former case has received a lot of attention in recent years, the latter has not been considered, to our knowledge. We address this question using a conservative dynamical system which has easily recognizable different dynamical behaviors (since there are no attractors) and two parameters whose variations lead to these behaviors. In this work, we investigate the dynamics of the standard nontwist map, which exhibits these properties. However, the kind of analysis we present in this paper can be applied to many other similar conservative systems with more than one parameter.

The nontwist maps have a peculiar behavior thanks to the nonmonotonicity of the winding number profile, and they do not obey KAM theory in all points of their phase space. The standard nontwist map has been the most intensively studied of all those systems and has two tunable parameters, whose variations lead to different dynamical behaviors. For selected values of these parameters we identify the presence, in the system two-dimensional phase space, of shearless invariant curves that act as barriers of transport throughout the chaotic area-filling orbits. For some values of these system parameters there occurs the breakup of these shearless curves. After this breakup there can be trajectories asymptoting both in the positive and negative directions in the transversal variable (the longitudinal value being periodic in the cylindrical phase space of the system).

The parameter space of these two variables is divided in two regions: parameter values for which there is a shearless barrier and for which there is escape through positive or negative values. We obtain the boundary between such behaviors using the method of indicator points. The form of this boundary suggests a self-similar structure, but in our work we demonstrate the fractal nature of this boundary, which is a representative example of fractal structure in the parameter space of a conservative dynamical system.

We have used two methods to achieve this conclusion: first the uncertainty dimension of the boundary has been determined to be *circa* 1.8. We know, however, that there are nonfractal (smooth) parts of the boundary (dimension equal

to the unity), which correspond to bifurcation curves already described by Wurm and co-workers [32]. The existence of two different dimensions depending on the region of the structure considered has been long known to occur in the phase space of dissipative dynamical systems. Hence, on the basis of the calculation we did, we cannot say that the value of ∼1.8 is the dimension of the fractal part, but instead it is the dimension of the boundary as a whole. While the boundary is clearly partially fractal and smooth, the dimension of the fractal part may not be the same as the uncertainty dimension of the boundary as a whole.

Moreover, this value is consistently the same in different regions of the boundary, suggesting that it is a homogeneous fractal structure. The second method was the computation of the basin entropy and basin boundary entropy, which quantify the uncertainty of the final state of any dynamical system. We obtained values of ∼0.05 for the basin entropy and ∼0.45 for the basin boundary entropy, which are also characteristic of a complicated fractal basin structure.

The method of uncertainty exponent we have used to estimate the dimension of the boundary in the parameter space allows us to estimate the final-state uncertainty issue raised by the fractality of the boundary. Using our estimate of 1.8 for the boundary dimension, the corresponding uncertainty exponent is $\alpha = 0.2$, such that the fraction of ε-uncertain conditions in the parameter space scales as $f(\varepsilon) \sim \varepsilon^{0.2}$. Suppose that we improve our determination of the parameter values (either a or b, or both) such that the uncertainty can be decreased at half its original value, i.e., $\varepsilon \to \varepsilon' = \varepsilon/2$. The fraction of ε-uncertain parameters will decrease to just $f' \sim 0.87 f$.

Hence a substantial reduction in the uncertainty of the parameters will not result in a proportional reduction in the fraction of uncertain parameters. The more α approaches zero the more unfavorable is this reduction. In the limiting case of $\alpha \approx 0$ the fraction will not decrease at all. Hence it is increasingly difficult to reduce final-state uncertainty when one has a fractal boundary, which is an important issue if the map parameters are to be fed with experimentally obtained values, which are always known within a given confidence interval.

Notice that, in the case of conservative systems, we refer to a behavior basin: either the shearless barrier curve is or is not broken. Other qualitatively different behaviors could be similarly analyzed. We consider another example of nontwist map, the so-called quartic nontwist map, and found essentially the same behavior, showing that fractal boundaries may be quite common in the parameter space of conservative systems.

ACKNOWLEDGMENTS

We are indebted to Dr. Alex Wurm for many useful discussions and valuable suggestions. This work has been supported by grants from the Brazilian Government Agencies CAPES, CNPq, and Fundação de Amparo à Pesquisa do Estado de São Paulo (FAPESP, Brazil), under Grant No. 2018/03211-6.

[1] J. Aguirre, R. L. Viana, and M. A. F. Sanjuán, Rev. Mod. Phys. **81**, 333 (2009).
[2] C. Grebogi, S. W. McDonald, E. Ott, and J. A. Yorke, Phys. Lett. A **99**, 415 (1983).
[3] S. W. McDonald, C. Grebogi, E. Ott, and J. A. Yorke, Physica D **17**, 125 (1985).
[4] C. Grebogi, E. Ott, S. Pellikan, and J. A. Yorke, Physica D **13**, 261 (1984).
[5] S. Bleher, C. Grebogi, E. Ott, and R. Brown, Phys. Rev. A **38**, 930 (1988).
[6] Y.-T. Lau, J. M. Finn, and E. Ott, Phys. Rev. Lett. **66**, 978 (1991).
[7] F. C. Moon, Phys. Rev. Lett. **53**, 962 (1984).
[8] P. Cvitanović, M. H. Jensen, L. P. Kadanoff, and I. Procaccia, Phys. Rev. Lett. **55**, 343 (1985).
[9] B. V. Chirikov, Phys. Rep. **52**, 263 (1979).
[10] M. Hénon and C. Heiles, Astron. J. **69**, 73 (1964).
[11] F. Blesa, J. Seoane, R. Barrio, and M. A. F. Sanjuán, Int. J. Bifur. Chaos **22**, 1230010 (2012).
[12] D. del Castillo-Negrete and P. J. Morrison, Phys. Fluids A **5**, 948 (1993).
[13] G. A. Oda and I. L. Caldas, Chaos, Solitons Fractals **5**, 15 (1995).
[14] R. Balescu, Phys. Rev. E **58**, 3781 (1998).
[15] D. del Castillo-Negrete, J. M. Greene, and P. J. Morrison, Physica D **91**, 1 (1996).
[16] D. del Castillo-Negrete, J. M. Greene, and P. J. Morrison, Physica D **100**, 311 (1997).
[17] A. Wurm, A. Apte, and P. J. Morrison, Braz. J. Phys. **34**, 1700 (2004).
[18] J. Aguirre, J. C. Vallejo, and M. A. F. Sanjuán, Phys. Rev. E **64**, 066208 (2001).
[19] T. Kovács and B. Érdi, Astron. Nach. **328**, 801 (2007).
[20] T. Uzer and D. Farrelly, Phys. Rev. A **52**, R2501(R) (1995).
[21] J. S. Portela, I. L. Caldas, R. L. Viana, and M. A. F. Sanjuán, Int. J. Bifurcat. Chaos **17**, 4067 (2007).
[22] A. C. Mathias, R. L. Viana, T. Kroetz, and I. L. Caldas, Physica A **469**, 681 (2017).
[23] A. Daza, A. Wagemakers, B. Georgeot, D. Guéry-Odelin, and M. A. F. Sanjuán, Sci. Rep. **6**, 31416 (2016).
[24] A. Daza, B. Georgeot, D. Guéry-Odelin, A. Wagemakers, and M. A. F. Sanjuán, Phys. Rev. A **95**, 013629 (2017).
[25] A. C. Mathias, T. Kroetz, I. L. Caldas, and R. L. Viana, Chaos Solitons Fractals **104**, 588 (2017).
[26] A. Gusso, R. L. Viana, A. C. Mathias, and I. L. Caldas, Chaos Solitons Fractals **122**, 6 (2019).
[27] R. S. MacKay, J. D. Meiss, and I. C. Percival, Phys. Rev. Lett. **52**, 697 (1984).
[28] D. Blazevski and D. del-Castillo-Negrete, Phys. Rev. E **87**, 063106 (2013).
[29] M. Mugnaine, A. C. Mathias, M. S. Santos, A. M. Batista, J. D. Szezech, Jr., and R. L. Viana, Phys. Rev. E **97**, 012214 (2018).
[30] S. Shinohara and Y. Aizawa, Prog. Theor. Phys. **97**, 379 (1997).

[31] S. Shinohara and Y. Aizawa, Prog. Theor. Phys. **100**, 219 (1998).
[32] A. Wurm, A. Apte, K. Fuchss, and P. J. Morrison, Chaos **15**, 023108 (2005).
[33] C. Grebogi, E. Kostelich, E. Ott, and J. A. Yorke, Physica D **25**, 347 (1987).
[34] A. Apte, A. Wurm, and P. J. Morrison, Chaos **13**, 421 (2003).
[35] E. Petrisor, J. H. Misguich, and D. Constantinescu, Chaos Solitons Fractals **18**, 1085 (2003).
[36] P. Menck, J. Heitzig, N. Marwan, and J. Kurths, Nat. Phys. **9**, 89 (2013).
[37] P. Menck, J. Heitzig, J. Kurths, and H. J. Schellnhuber, Nat. Commun. **5**, 3969 (2014).
[38] A. Wurm and K. Fuchss Portela, Commun. Nonlin. Sci. Numer. Simulat. **17**, 2215 (2012).